Controlled Interconversion of Superposed-Bistriangle, Octahedron, and Cuboctahedron Cages Constructed Using a Single, Terpyridinyl-based Polyligand and Zn^{2+}

Ting-Zheng Xie,† Kevin J. Endres,‡ Zaihong Guo,‡ James M. Ludlow III,† Charles N. Moorefield,† Mary Jane Saunders,# Chrys Wesdemiotis*,†,‡ and George R. Newkome*,†,‡

Experimental Section

General Procedures. Reagents and solvents were purchased from Sigma-Aldrich and used without purification. 4,4',5,5'-Tetrabromodibenzo-18-crown-6 was synthesized according to the literature.[S1] Thin layer chromatography (TLC) was performed on flexible sheets (Baker-flex) precoated with Al_2O_3 (IB-F) or SiO_2 (IB2-F) and visualized by UV light. Column chromatography was conducted using basic Al_2O_3, Brockman Activity I (60-325 mesh) or SiO_2 (60-200 mesh) from Fisher Scientific. ^1H, ^{13}C, 2D COSY, and NOESY NMR spectra were recorded on a Varian 500 MHz NMR. ESI mass spectrometry (MS) experiments were performed on a Waters Synapt HDMS quadrupole/time-of-flight (Q/ToF) tandem mass spectrometer. This instrument contains a triwave device between the Q and ToF analyzers, consisting of three collision cells in the order: trap cell, ion mobility cell, and transfer cell. Trap and transfer cells were pressurized with Ar, and the ion mobility cell was pressurized with N_2 flowing in a direction opposite to that of the entering ions. In TWIM experiments, a pulsed field was applied to the ion mobility cell ("traveling wave" field) to separate the ions drifting inside it by their charge state and collision cross-section. MALDI-ToF-MS measurements were performed with a Bruker UltraFlex III ToF/ToF instrument, equipped with a Nd:YAG laser emitting at a wavelength of 355 nm. The proteins used to calibrate the drift time scale in TWIM-MS experiments in order to obtain collision cross-sections were acquired from Sigma-Aldrich. The ESI-TWIM-MS experiments were performed using the following parameters: ESI capillary voltage: 1.0 kV; sample cone voltage: 8 V; extraction cone voltage: 3.2 V; desolvation gas flow: 800 L h^{-1}(N_2); trap collision energy (CE): 1 eV; transfer CE: 1 eV; trap gas flow: 1.5 mL min^{-1} (Ar); ion-mobility cell gas flow: 22.7 mL min^{-1} (N_2); sample flow rate: 5μL min^{-1}; source temperature: 30 °C; desolvation temperature: 40 °C; TWIM traveling-wave height: 7.5 V; and TWIM traveling-wave velocity: 350 ms^{-1}. The sprayed solution was prepared by dissolving the sample (300 μg) in a mixture of MeCN/MeOH (1 mL; 1:1, v/v). Data analyses were conducted using the MassLynx 4.1 and DriftScope 2.1 programs provided by Waters. Theoretical collision cross sections were calculated from energy minimized structures using the trajectory method available in the

MOBCAL software. For the TEM investigation, the sample was dissolved in MeCN at a concentration within the range 10^{-6} to 10^{-7} M. The solutions were drop cast onto a carbon-coated copper grid and extra solution was absorbed by filter paper to avoid aggregation. The TEM images of the drop cast samples were taken with a Jeol JEM-1230 transmission electron microscope.

Collision Cross-Section Calibration. The drift time scale of the TWIM-MS experiments was converted to a collision cross-section scale following the calibration procedure of Scrivens, *et al*.[S2] Briefly, the corrected collision cross sections of the molecular ions of insulin (bovine pancreas), ubiquitin (bovine red blood cells), and cytochrome C (horse heart), obtained from published work,[S3] were plotted against the corrected drift times (arrival times) of the corresponding molecular ions measured in TWIM-MS experiments at the same traveling-wave velocity, traveling-wave height, and ion-mobility gas flow settings, *viz*. 350 ms^{-1}, 7.5 V and 22.7 mL min^{-1}. All charge states observed for the calibrants were used in the construction of the curve.

Molecular Modeling. Energy minimization of the macrocycles was conducted with the Materials Studio version 6.0 program, using the Anneal and Geometry Optimization tasks in the Forcite module (Accelrys Software, Inc.). The counterions were omitted. An initially energy-minimized structure was subjected to 100 anneal cycles with initial and mid-cycle temperatures of 300 and 1500 K, respectively, twenty heating ramps per cycle, one thousand dynamics steps per ramp, and one dynamics step per femtosecond. A constant volume/constant energy (NVE) ensemble was used; the geometry was optimized after each cycle. All geometry optimizations used a universal force field with atom-based summation and cubic spline truncation for both the electrostatic and van der Waals parameters. For each metallocage, 100 candidate structures were generated for the calculation of the collision cross-sections.

4,4',5,5'-Tetra*kis*(4-terpyridinylphenyl)dibenzo-18-crown-6 (3). A mixture of 4,4',5,5'-tetrabromodibenzo-18-crown-6[S1] (676.0 mg, 1 mmol), 4'-(4-boronatophenyl)-2,2':6',2"-terpyridine[S4] (2.12 g, 6 mmol), Na_2CO_3 (840 mg, 10 mmol), and $Pd(PPh_3)_2Cl_2$ (210.5 mg, 0.3 mmol) in a solution of MeOH (80 mL), H_2O (120 mL), and toluene (200 mL) was refluxed for 48 h under Ar. After separating the toluene layer, the aqueous layer was extracted with $CHCl_3$ (150 mL, 3X). The combined organic layer was dried ($MgSO_4$), and concentrated *in vacuo*. The residue was column chromatographed eluting with a hexane, $CHCl_3$, and EtOAc (2:1:1) mixture and then pure $CHCl_3$, which gave **3**, as a pale yellow powder: 747.1 mg (47%); m.p.: 338.4-339.2 °C (dec); ^{1}H NMR (500 MHz, $CDCl_3$, 300 K, Figure S1) δ 8.73 (s, 8H, tpy$H^{3',5'}$), 8.68 (d, $J_{6,6"-5,5"}$ = 6 Hz, 8H, tpy$H^{6,6"}$), 8.63 (d, $J_{3,3"-4,4"}$ = 10 Hz, 8H, tpy$H^{3,3"}$), 7.84 (m, 8H, tpy$H^{4,4"}$), 7.79 (d, J_{a-b} = 10 Hz, 8H, Ph*a*), 7.31 (m, 8H, tpy$H^{5,5"}$), 7.30 (d, J_{b-a} = 10 Hz, 8H, Ph*b*), 7.05 (s, 4H, Ph*c*), 4.32 (t, 8H, CH_2), 4.01 (t, 8H, CH_2), 3.92 (s, 8H, CH_2); ^{13}C NMR (125 MHz, $CDCl_3$, 300 K, Figure S2) 156.18, 155.80, 149.96, 148.92, 148.38, 142.34, 137.23, 136.16, 133.11, 130.64, 126.92, 123.94, 121.71, 118.87, 116.22, 70.01, 69.25; MALDI-TOF [M + H^+] 1590.71, calcd. 1589.83.

Complex (4) with PF_6^-. To the solution of tetra*kis*terpyridinyl ligand **3** (11.7 mg, 8 μmol) in $CHCl_3$ and MeOH (1:1, 16 mL) was added a MeOH (1 mL) solution of $Zn(NO_3)_2 \cdot 6H_2O$ (4.8 mg, 16 μmol) slowly. The mixture was stirred at 25 ºC for 2h, then 10-fold excess NH_4PF_6 was added. The residue was filtered, washed with water (10 mL × 3) and MeOH (10 mL × 3), and then dried *in vacuo* to give complex **4**, as a yellow solid: 18 mg (98%): m.p. >400 °C; ^{1}H NMR (500 MHz, DMF-d_7, 300 K, ppm, Figure S3) for the cuboctahedron: δ 9.46 (s, 96H, tpy$H^{3',5'}$), 9.18 (d, $J_{3,3"-4,4"}$ = 9 Hz, 96H, tpy$H^{3,3"}$), 8.45 (d, J_{a-b} = 12 Hz, 96H, Ph*a*), 8.24 (m, 96H, tpy$H^{4,4"}$), 8.18 (d, $J_{6,6"-5,5"}$ = 6 Hz, 96H, tpy$H^{6,6"}$), 7.70 (d, J_{b-a} = 12 Hz, 96H, Ph*b*), 7.50 (m, 96H, tpy$H^{5,5"}$), 7.30 (s, 48H, Ph*c*), 4.48 (broad peak, 48H, CH_2*d*), 4.45 (broad peak, 48H, CH_2*e*), 4.21 (broad peak, 48H, CH_2*d*'), 4.00 (broad peak, 48H, CH_2*e*'); ^{13}C NMR (125 Hz, DMSO-d_6, 300 K, ppm, Figure S4): δ 162.75, 154.59, 154.34, 151.15, 149.92, 148.12, 144.41, 141.78, 139.71, 133.56, 131.39, 128.15, 123.93, 120.89, 119.79, 36.23, 31.24; MS see Figure S15

(with PF_6^- in MeCN and DMSO).

Complex (5) with PF_6^-: Dilution of the DMSO-d_6 solution of complex **4** (1 mg/mL) with CD_3CN to 0.1 mg/mL gave octahedron complex **5**, as a mixture. For the octahedron **5** (PF_6^-): ^{1}H NMR (500 MHz, DMSO-d_6/CD_3CN (v/v 1:10), 300 K, ppm, Figure S5): δ 9.01 (s, 96H, tpy$H^{3',5'}$), 8.75 (d, $J_{3,3''\text{-}4,4''}$ = 8 Hz, 96H, tpy$H^{3,3''}$), 8.17 (d, $J_{a\text{-}b}$ = 8 Hz, 96H, Ph*a*), 8.12 (m, 96H, tpy$H^{4,4''}$), 7.87 (d, $J_{6,6''\text{-}5,5''}$ = 5 Hz, 96H, tpy$H^{6,6''}$), 7.65 (d, $J_{b\text{-}a}$ = 8 Hz, 96H, Ph*b*), 7.38 (m, 96H, tpy$H^{5,5''}$), 7.28 (s, 48H, Ph*c*), 4.43 (broad peak, 48H, CH_2*d*), 4.38 (broad peak, 48H, CH_2*e*), 4.19 (broad peak, 48H, CH_2*d*'), 3.99 (broad peak, 48H, CH_2*e*'). For the MS see Figure S13 (PF_6^- in MeCN and DMSO, concentration 0.05 mg/mL).

Superposed-*bis*triangular complex 6 with PF_6^-: Dilution of the DMF-d_7 solution of complex **4** (1 mg/mL) with CD_3CN to 0.5 μg/mL gave a mixture of octahedron complex **5** along with **6**: ^{1}H NMR (500 MHz, DMSO-d_6/CD_3CN (v/v, 1:10), 300K, ppm, Figure S5): δ 8.98 (s, 96H, tpy$H^{3',5'}$), 8.71 (d, $J_{3,3''\text{-}4,4''}$ = 8 Hz, 96H, tpy$H^{3,3''}$), 8.14 (d, $J_{a\text{-}b}$ = 8 Hz, 96H, Ph*a*), 8.10 (m, 96H, tpy$H^{4,4''}$), 7.82 (d, $J_{6,6''\text{-}5,5''}$ = 5 Hz, 96H, tpy$H^{6,6''}$), 7.62 (d, $J_{b\text{-}a}$ = 8 Hz, 96H, Ph*b*), 7.38 (m, 96H, tpy$H^{5,5''}$), 7.24 (s, 48H, Ph*c*), 4.43 (broad peak, 48H, CH_2*d*), 4.38 (broad peak, 48H, CH_2*e*), 4.19 (broad peak, 48H, CH_2*d*'), 3.99 (broad peak, 48H, CH_2*e*').

Complex 4 with BPh_4^- counter ions: Following the same procedure with complex **4**, with NH_4PF_6 replaced by $NaBPh_4$. m.p. >400 °C. For the cuboctahedron: ^{1}H NMR (500 MHz, CD_3CN/DMSO-d_6 (v/v, 4:1), 300 K, ppm) δ 9.00 (s, 48H, tpy$H^{3',5'}$), 8.57 (d, $J_{3,3''\text{-}4,4''}$ = 8 Hz, 48H, tpy$H^{3,3''}$), 8.20 (d, $J_{a\text{-}b}$ = 7 Hz, 48H, Ph*a*), 7.88 (m, 48H, tpy$H^{4,4''}$), 7.72 (d, 48H, tpy$H^{6,6''}$), 7.63 (s, 24H, Ph*c*), 7.25 (d, $J_{b\text{-}a}$ = 7 Hz, 48H, Ph*b*), 7.13 (m, 48H, tpy$H^{5,5''}$), 7.20 (broad peak, 192H, PhB$^-H^f$), 6.87 (t, 192H, PhB$^-H^g$), 6.73 (t, 96H, PhB$^-H^h$), 4.44 (broad peak, 48H, CH_2*d*), 4.34 (broad peak, 48H, CH_2*e*), 4.16 (broad peak, 48H, CH_2*d*'), 3.94 (broad peak, 48H, CH_2*e*'); ESI-MS Figure S10 (MeCN and DMSO).

Complex 6 with BPh_4^- counter ions: Dilution of the DMSO-d_6 solution of complex **4** (1 mg/mL) with CD_3CN to 5 µg/mL gave the mixture of superposed-*bis*triangular complex **6**: ^{1}H NMR (500 MHz, CD_3CN/DMSO-d_6 (v/v, 4:1), 300 K, ppm, Figure 1d) δ 8.74 (s, 48H, tpy$H^{3',5'}$), 8.27 (d, $J_{3,3''\text{-}4,4''}$ = 8 Hz, 48H, tpy$H^{3,3''}$), 8.03 (d, $J_{a\text{-}b}$ = 7 Hz, 48H, PhH^{a}), 7.79 (m, 48H, tpy$H^{4,4''}$), 7.60 (d, $J_{6,6''\text{-}5,5''}$ = 7 Hz, 48H, tpy$H^{6,6''}$), 7.37 (s, 24H, PhH^{c}), 7.19 (d, $J_{b\text{-}a}$ = 7 Hz, 48H, PhH^{b}), 7.19 (broad peak, 192H, PhB^--H^{f}), 6.85 (t, 192H, PhB^--H^{g}), 7.06 (m, 48H, tpy$H^{5,5''}$), 6.71 (t, 96H, PhB^--H^{h}), 4.42 (broad peak, 48H, CH_2d), 4.33 (broad peak, 48H, CH_2e), 4.15 (broad peak, 48H, CH_2d'), 3.93 (broad peak, 48H, CH_2e'); ESI-MS see Figure S11 (BPh_4^- in MeCN and DMSO, concentration 5 µg/mL); ESI-TWIM-MS see Figure S17 (BPh_4^- in MeCN and DMSO, concentration 0.05 mg/mL).

^{1}H & ^{13}C NMR and DOSY NMR of compounds 4 - 6

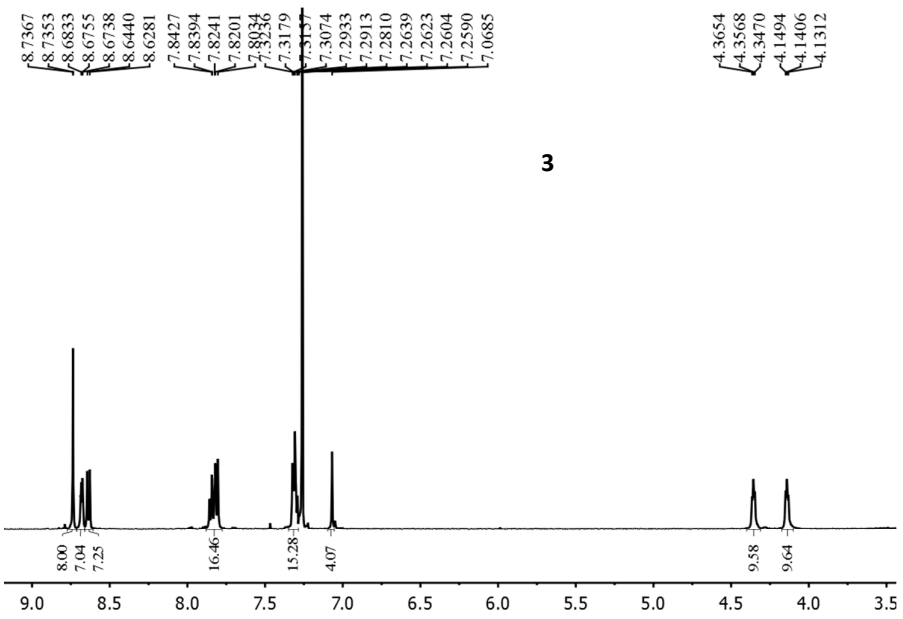

Figure S1. ^{1}H NMR spectrum of ligand **3** in $CDCl_3$ (300 K, 500 MHz)

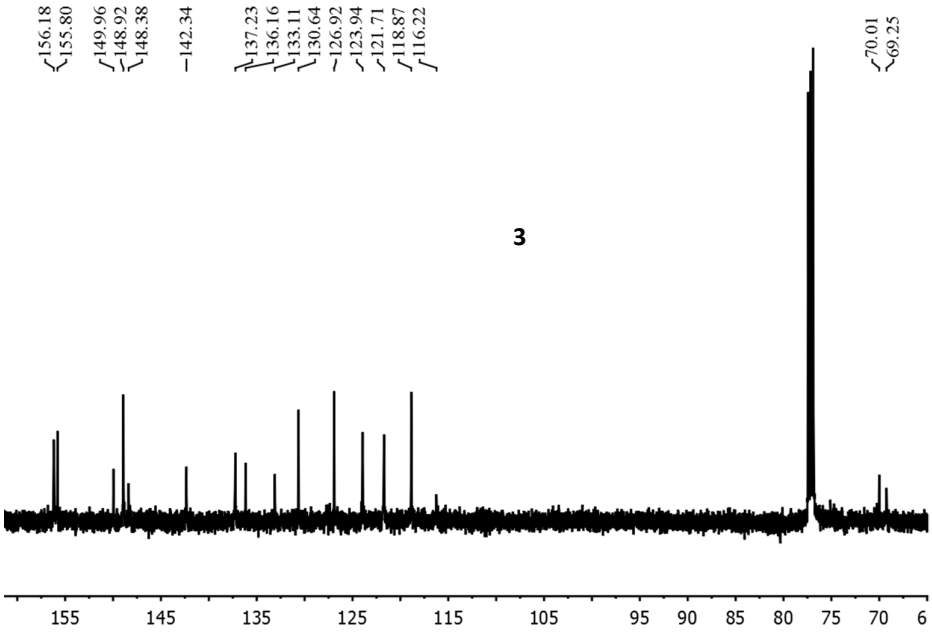

Figure S2. ^{13}C NMR spectrum of ligand **3** in $CDCl_3$/MeOD (5:1, v/v), 300 K, 125 MHz.

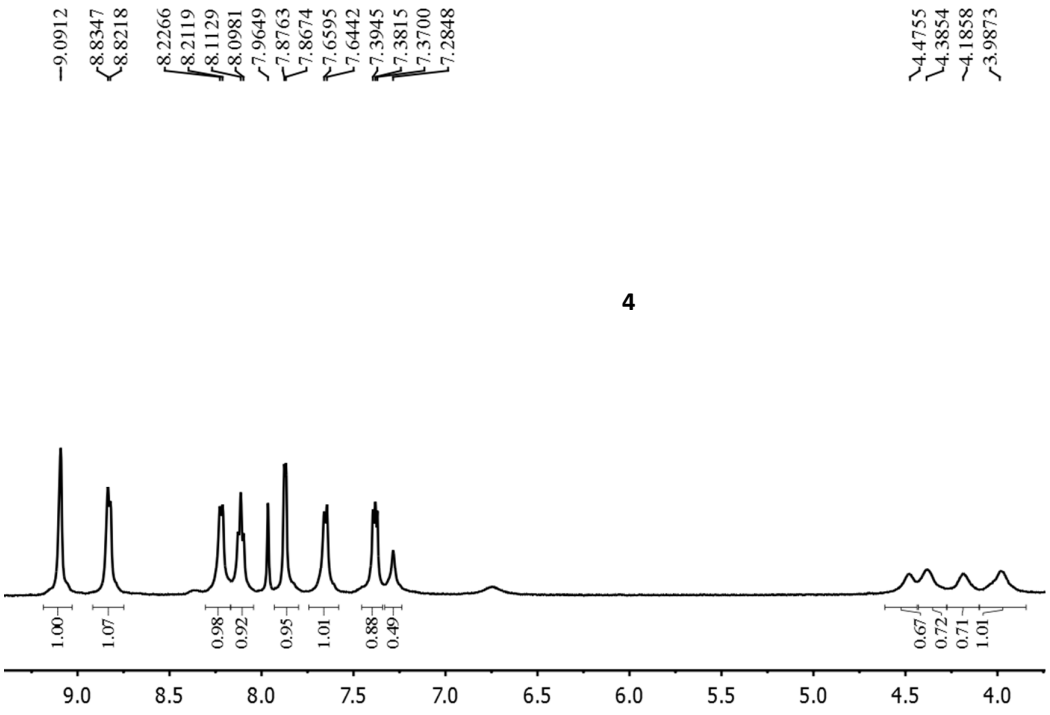

Figure S3. ^{1}H NMR spectrum of complex **4** in DMSO-d_6 (300 K, 500 MHz).

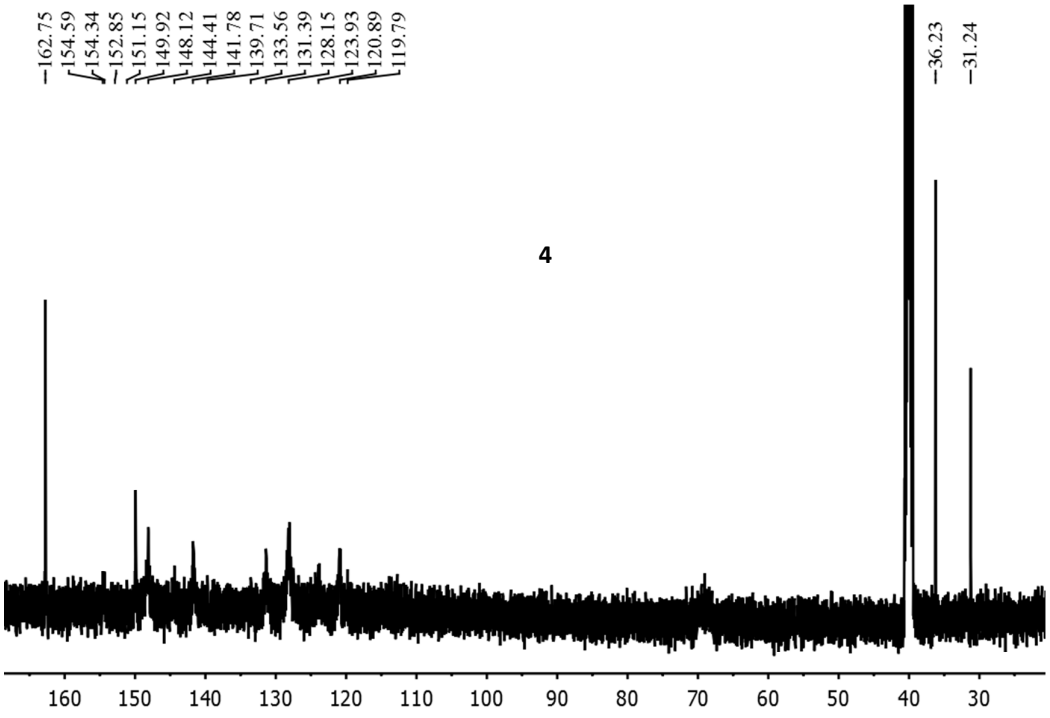

Figure S4. ^{13}C NMR spectrum of complex **4** in DMSO-d_6 (300 K, 125 MHz).

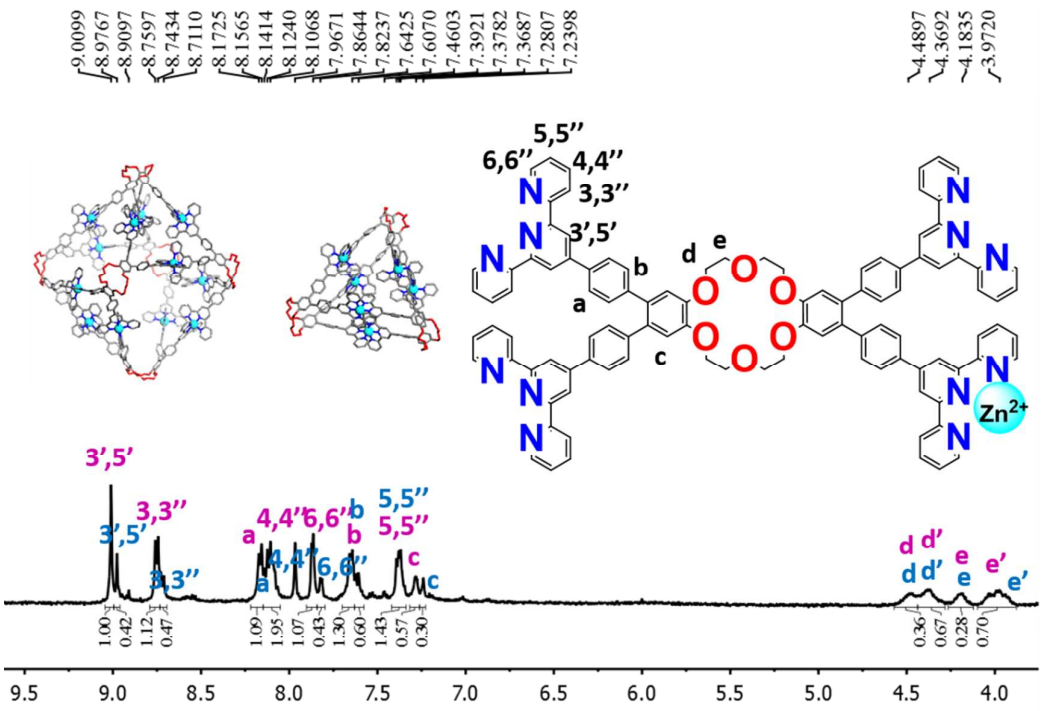

Figure S5. ^{1}H NMR spectrum of complexes **5** and **6** with PF_6^- anions in DMSO-d_6/CD_3CN (1:9) (300 K, 500 MHz). The spectrum suggests a mixture of octahedron and double triangle conformers (purple, octahedron; blue, double triangle).

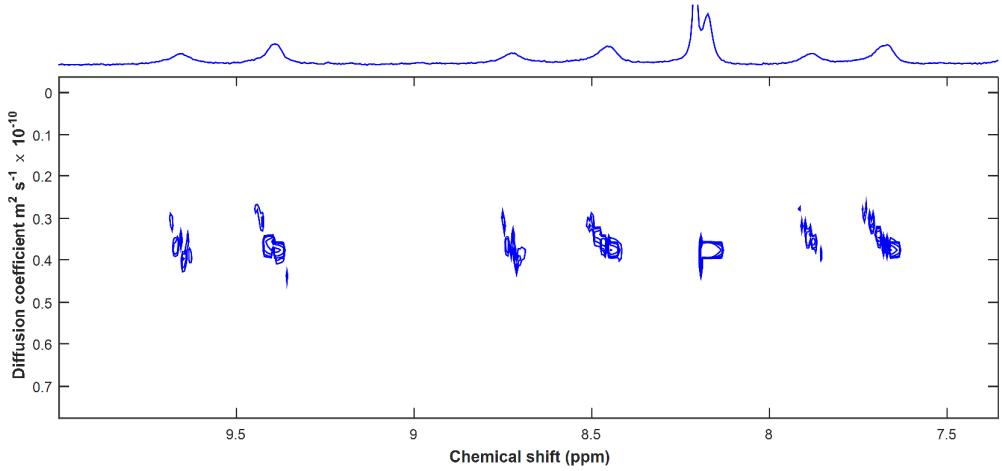

Figure S6. ^{1}H DOSY spectrum of **4** in DMSO-d_6 and CD_3CN (1:4, v/v).

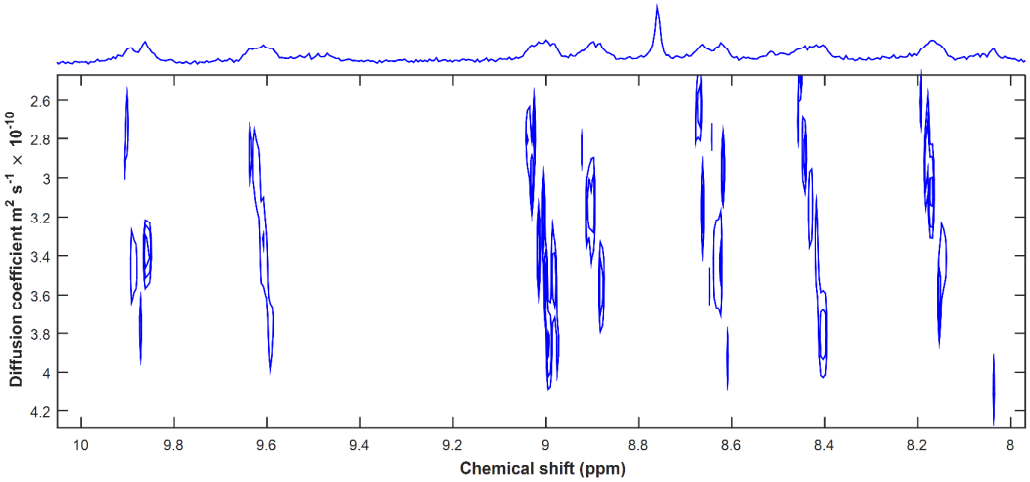

Figure S7. ^{1}H DOSY spectrum of the mixture **5** and **6** in DMSO-d_6 and CD_3CN (1:4, v/v).

The sphere hydrodynamic radius can be estimated, according to the Stokes-Einstein Equation. Where D is the diffusion constant, k is the Boltzmann's constant, T is the temperature, μ is the viscosity of solvents, and R is the radius of the sphere-like particles:

$$D = \frac{kT}{6\pi\mu R}$$

$D = 10^{-10.44}$ m^2 s^{-1}

$k = 1.38\times10^{-23}$ N m K^{-1}

$T = 298$ K

$\mu = 2.0\times10^{-3}$ N m^{-2} s (DMSO)

$R = \frac{kT}{6\pi\mu D} = 3.03\times10^{-9}$ m = 3.03 nm

The radius of the spherical complex **4** is 3.03 nm, complex **5** is 1.98 nm, and complex **6** is 1.40 nm, which are consistent with the results of computer modeling.

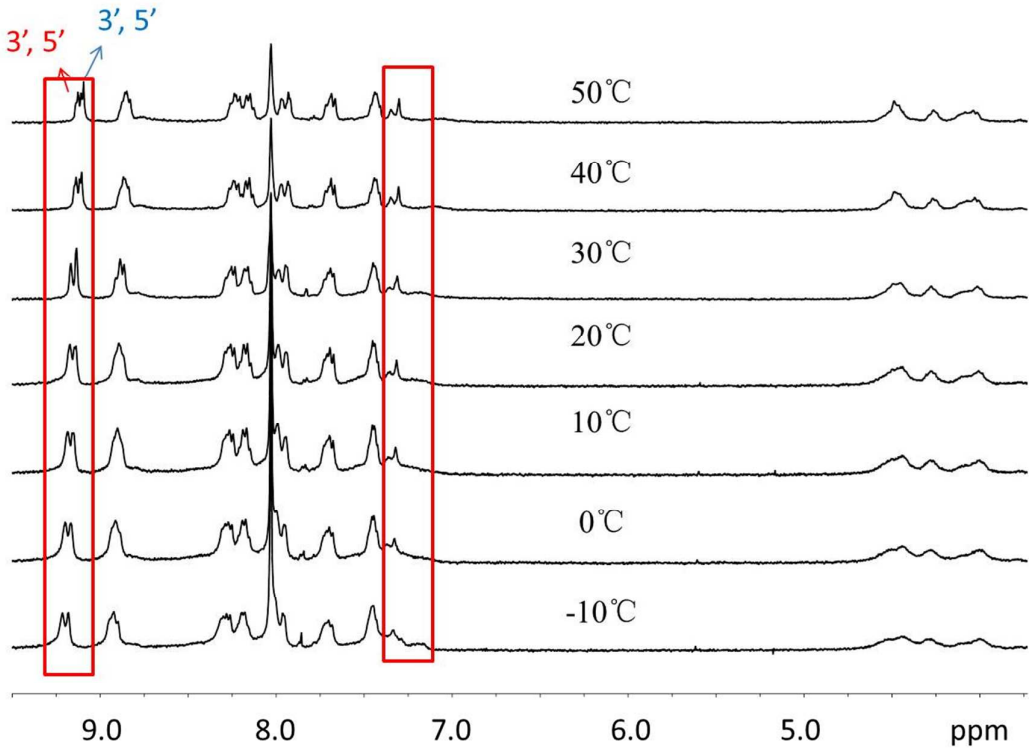

Figure S8. The variable temperature ^{1}H NMR spectra of mixture of complex **4** and complex **5** (concentration 0.4 mg/mL) [400 MHz, DMF-d_7/CD_3CN (v/v 1:5)].

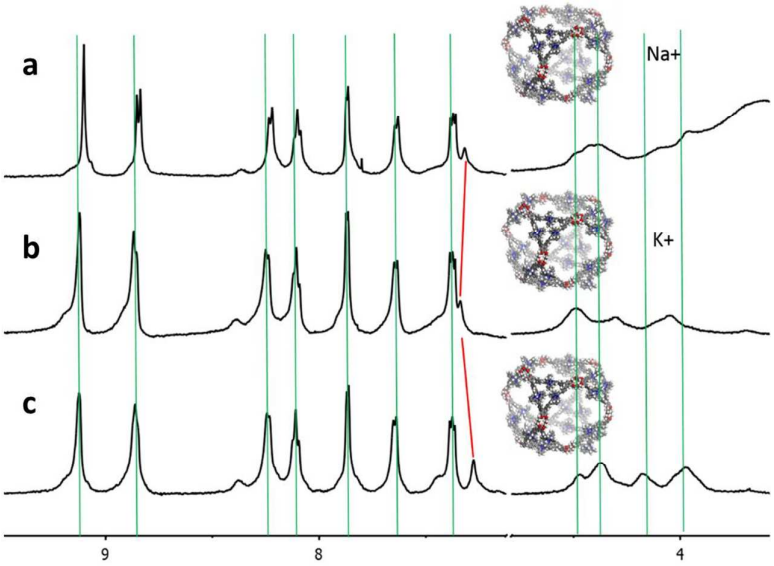

Figure S9. The ^{1}H NMR spectra of complex **4** with addition of excess a) Na^+, b) K^+, c) none.

ESI-MS spectra, TWIM spectra and UV-vis

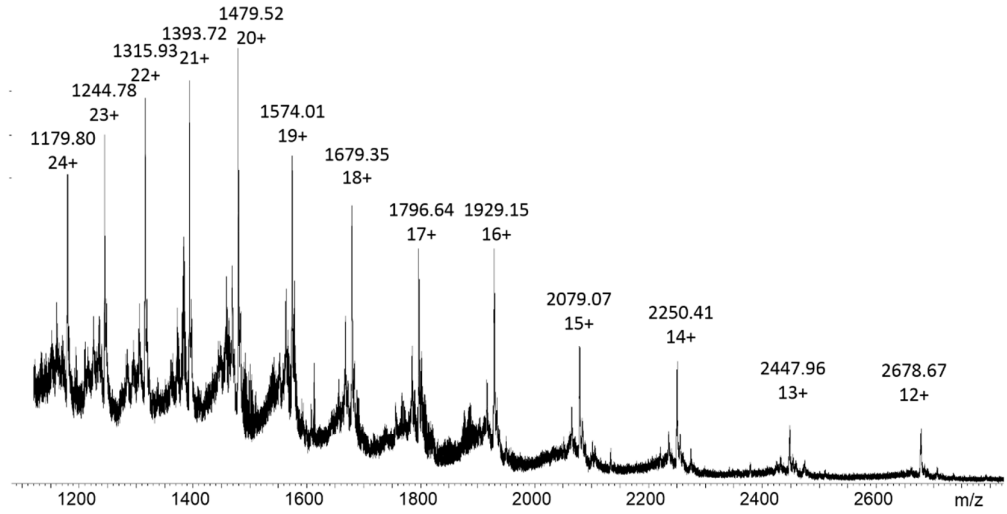

Figure S10. ESI-MS spectrum of complex **4** with BPh_4^- in MeCN and DMSO (concentration 0.5 mg/mL).

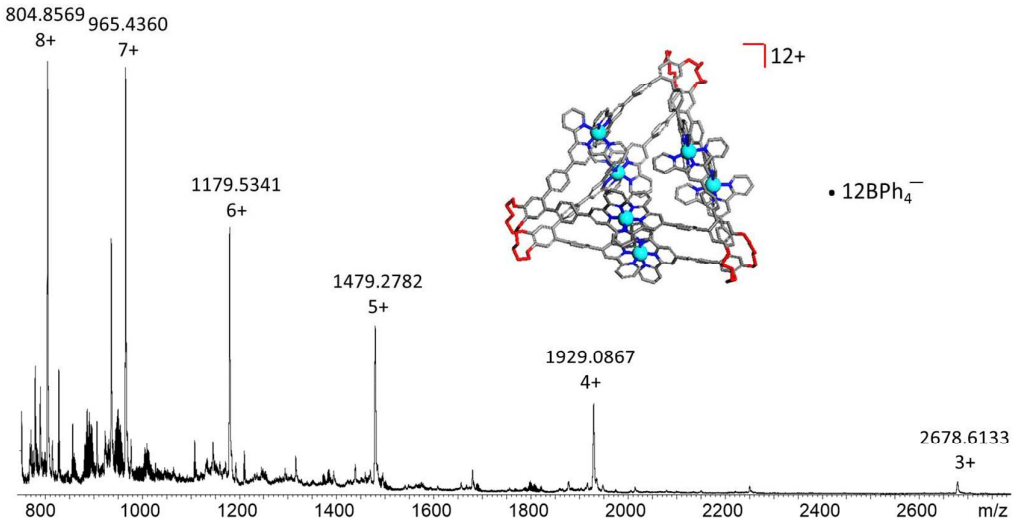

Figure S11. ESI-MS spectrum of complex **6** with BPh_4^- in MeCN and DMSO (concentration 5 µg/mL).

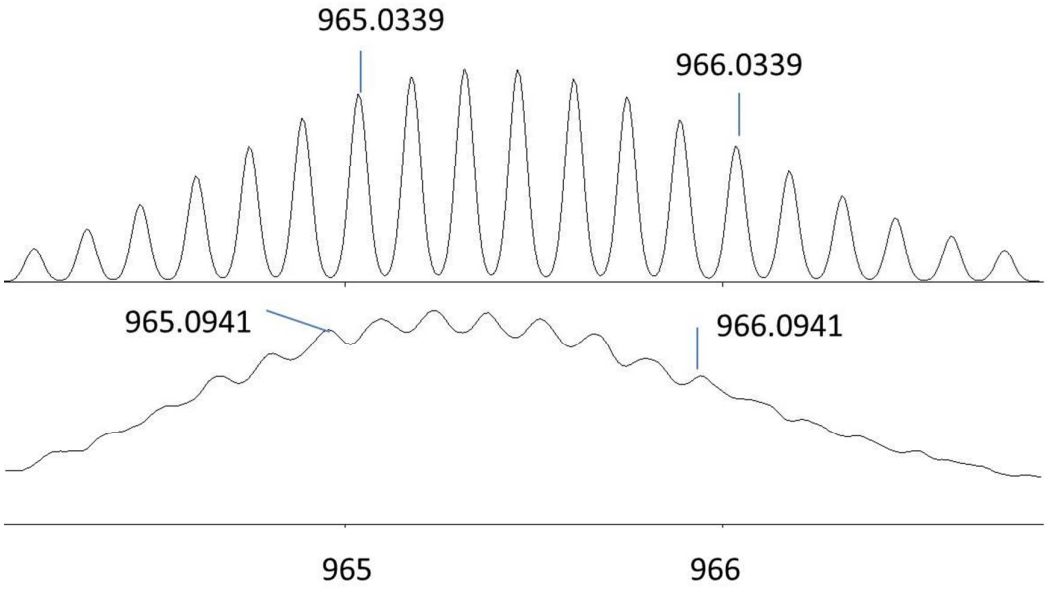

Figure S12. Isotopic distribution pattern and the simulated pattern of the +7 peaks in ESI-MS spectrum of complex **6**.

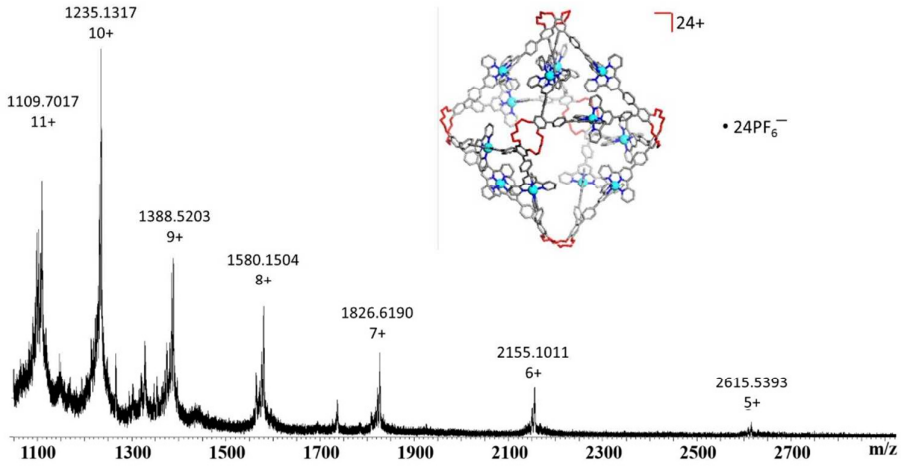

Figure S13. ESI-MS spectrum of complex **5** with PF_6^- in MeCN and DMSO (concentration 0.05 mg/mL).

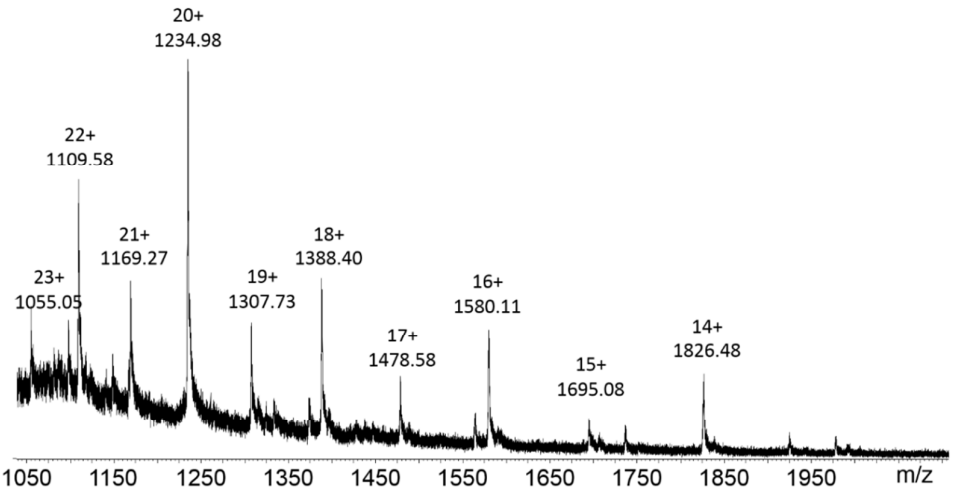

Figure S14. ESI-MS spectrum of complexes **4** and **5** in DMSO and MeCN (1:4 v/v).

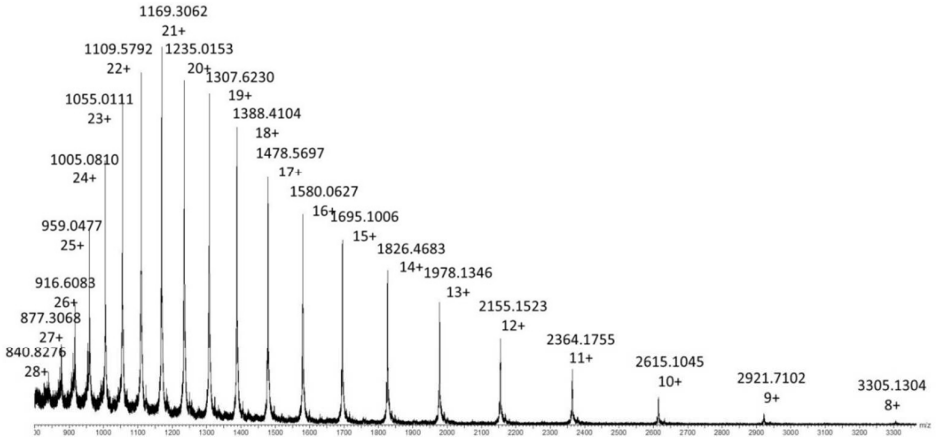

Figure S15. ESI-MS spectrum of cuboctahedron complex **4** in DMSO and MeCN (1:4 v/v).

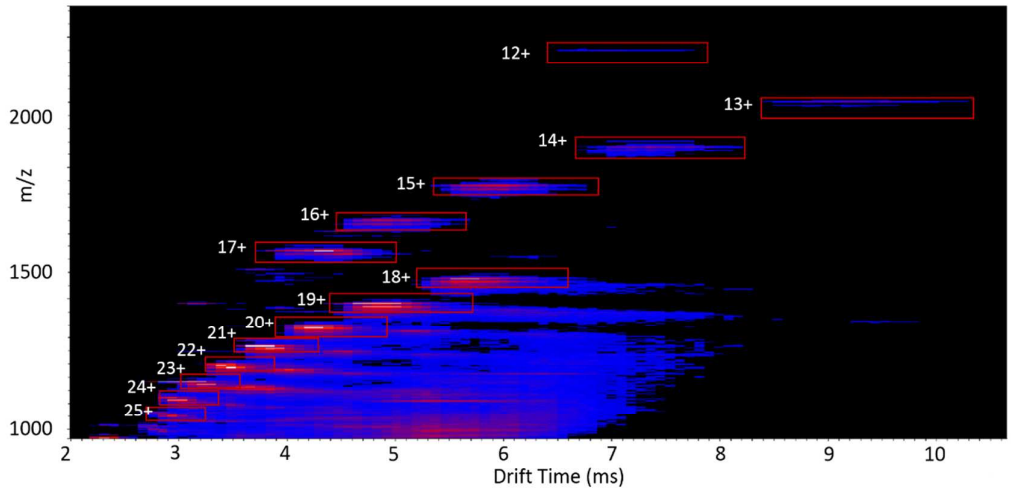

Figure S16. ESI-TWIM-MS spectrum of complex **4** with BPh_4^- in MeCN and DMSO (concentration 0.5 mg/mL).

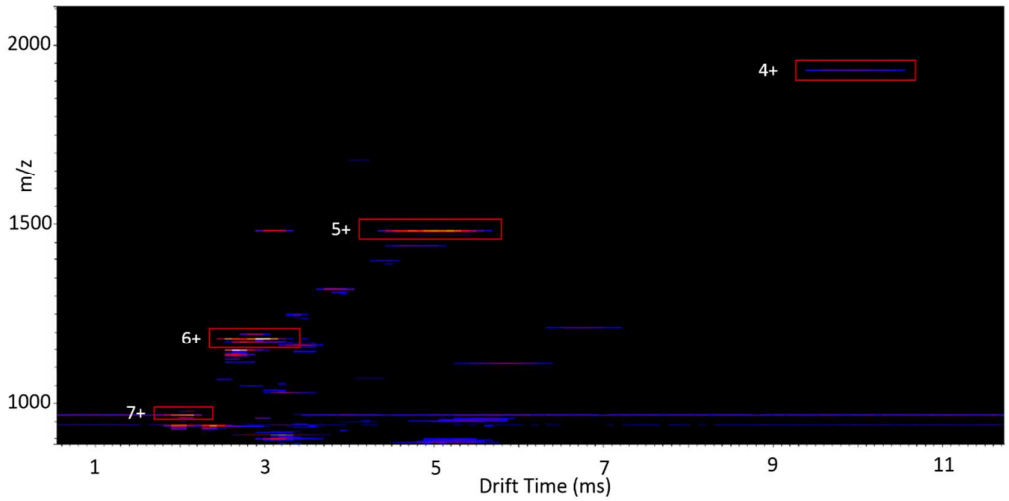

Figure S17. ESI-TWIM-MS spectrum of complex **6** with BPh_4^- in MeCN and DMSO (concentration 0.05 mg/mL).

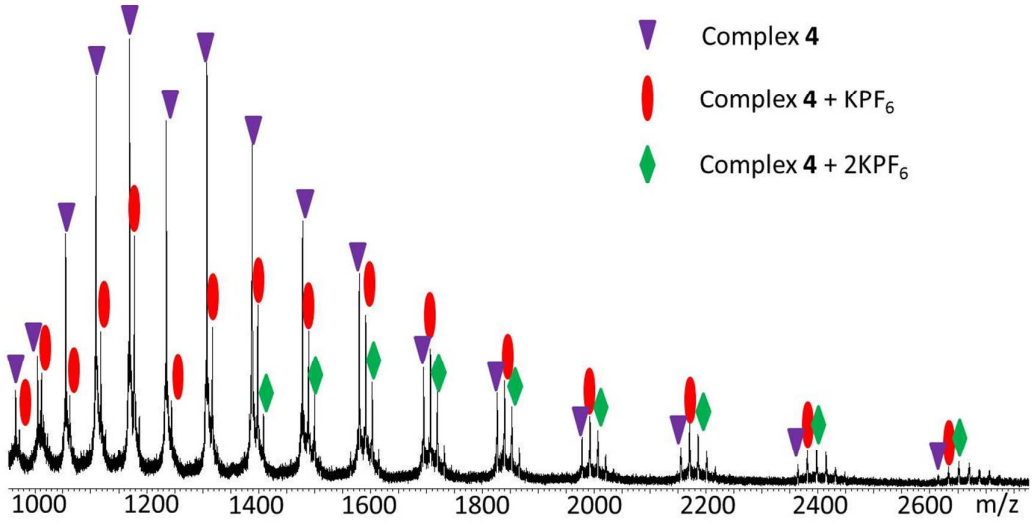

Figure S18. The ESI-MS spectrum of complex **4** with 12 eq KPF_6.

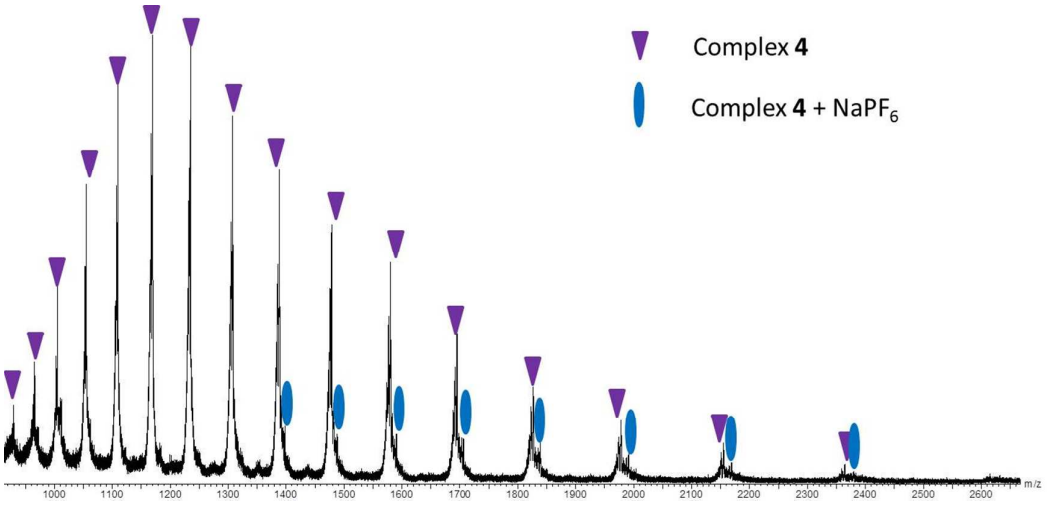

Figure S19. The ESI-MS spectrum of complex **4** with 12 eq $NaPF_6$.

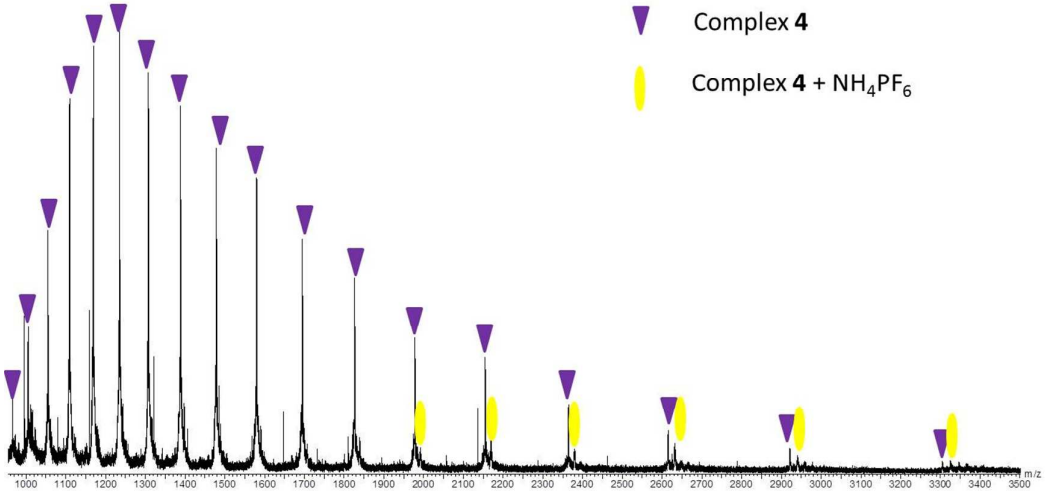

Figure S20. The ESI-MS spectrum of complex **4** with 12 eq NH_4PF_6.

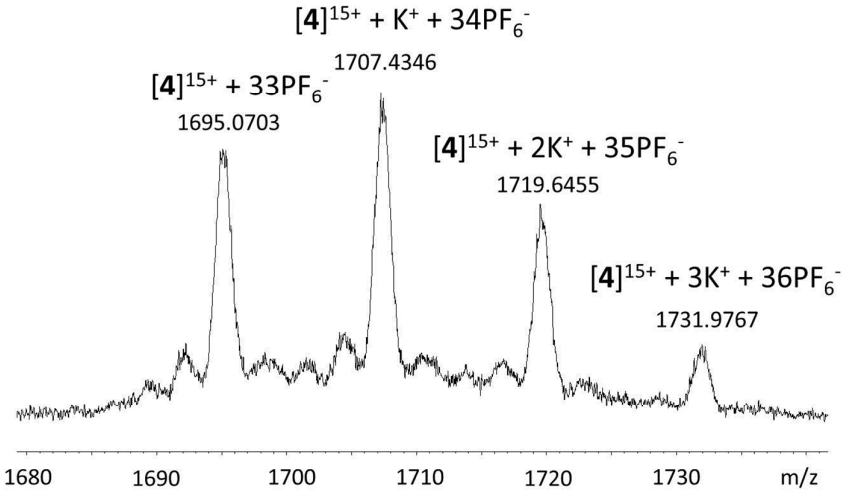

Figure S21. The spectrum of 15+ isotope of complex **4** with 12 eq KPF_6.

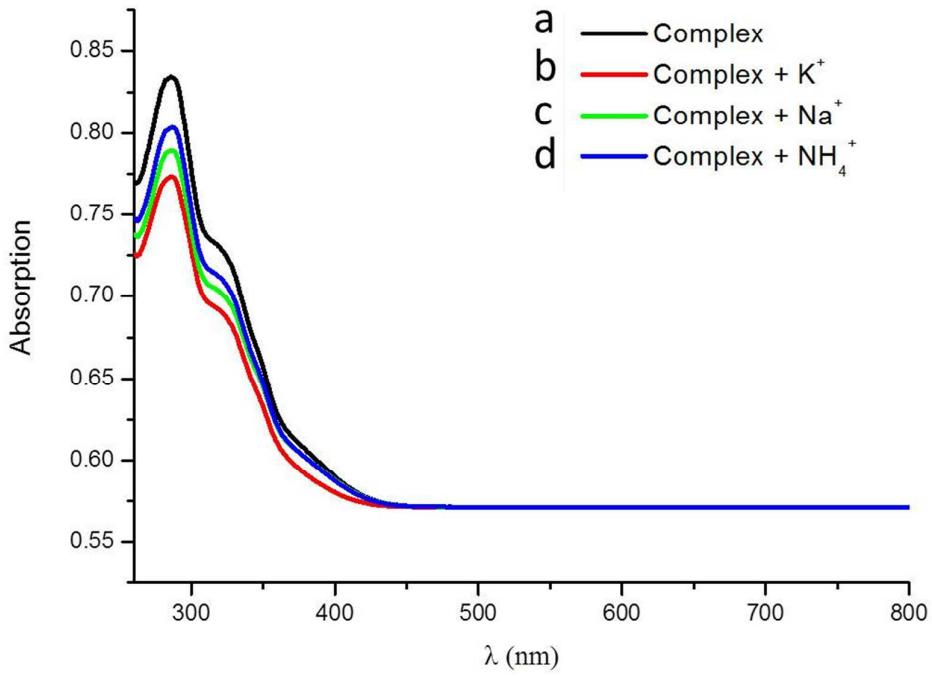

Figure S22. The UV-vis spectra of a) complex **6** (concentration 1.5 X 10^{-6} mmol/mL, black); b) complex X with 12 eq KPF_6 (red); c) complex X with 12 eq $NaPF_6$ (green); d) complex X with 12 eq NH_4PF_6 (blue).

Calibration of drift time scale and collision cross sections

Table S1. Experimental drift times (t_D)* and collision cross sections (CCS) for complex 4 with PF_6^-.

z	MW (Da)	m/z	t_D	Average CCS ($Å^2$)	Std. Dev. ($Å^2$)
10	26156.5	2615.65	9.93	1949.19	9.27
11	26009.61	2364.51	8.51	2116.91	17.77
12	25864.2	2155.35	6.80	2269.94	21.66
13	25719.98	1978.46	7.97	2039.08	3.75
14	25574.36	1826.74	6.35	2183.89	10.13
15	25431	1695.4	5.08	2335.03	14.32
16	25284	1580.25	5.29	2492.07	8.97
17	25138.75	1478.75	5.96	2155.03	4.77
17	25138.75	1478.75	4.45	2630.81	11.37
18	24996.06	1388.67	5.78	2261.42	10.15
19	24842.12	1307.48	4.93	2371.14	14.50
20	24671.8	1233.59	4.27	2480.88	17.68
21	24560.13	1169.53	3.79	2579.72	20.97
22	24416.04	1109.82	3.40	2662.85	20.64
23	24270.29	1055.23	3.10	2743.39	27.46
24	24125.52	1005.23	1.96	2808.70	15.12
Average Experimental Collision Cross Sections (CCS) ($Å^2$)				2380.00	±129.22
Theoretical Collision Cross Sections (CCS) ($Å^2$)				2320	

Table S2. Experimental Drift times (t_D)* and collision cross sections (CCS) for complex 5 with PF_6^-.

z	MW (Da)	m/z	t_D	Average CCS ($Å^2$)	Std. Dev. ($Å^2$)
5	13078.35	2615.67	14.35	839.20	20.77
6	12933.66	2155.61	8.93	1170.05	27.31
7	12786.13	1826.59	5.69	1605.84	24.71
8	12642.48	1580.31	3.94	2079.73	27.09
9	12496.77	1388.53	5.72	1598.71	14.94
10	12351.3	1235.13	4.39	1925.39	7.76
11	12208.35	1109.85	3.40	2305.10	32.94
Average Experimental Collision Cross Sections (CCS) ($Å^2$)				1646.29	±23.57
Theoretical Collision Cross Sections (CCS) ($Å^2$)				1598.60	

Table S3. Experimental Drift times (t_D)* and collision cross sections (CCS) for complex 4 with BPh_4^-.

z	MW (Da)	m/z	t_D	Average CCS ($Å^2$)	Std. Dev. ($Å^2$)
14	31505.74	2250.41	9.21	1961.61	11.74
15	31186.05	2079.07	7.38	2099.02	15.91
16	30866.4	1929.15	9.53	1940.80	2.81
16	30866.4	1929.15	5.83	2256.14	5.46
17	30542.88	1796.64	4.82	2391.27	6.88
18	30228.3	1679.35	4.24	2487.31	16.32
19	29906.19	1574.01	5.64	2279.06	16.81
20	29590.4	1479.52	4.77	2398.71	14.12
20	29590.4	1479.52	3.16	2723.61	24.00
21	29268.12	1393.72	4.27	2481.64	18.77
22	28950.46	1315.93	3.73	2587.13	29.18
23	28629.94	1244.78	3.37	2668.35	33.12
24	28315.2	1179.8	3.63	2608.58	6.38
Average Experimental Collision Cross Sections (CCS) ($Å^2$)				2375.63	±17.85
Theoretical Collision Cross Sections (CCS) ($Å^2$)				2320	

Table S4. Experimental Drift times (t_D)* and collision cross sections (CCS) for complex 6 with BPh_4^-.

z	MW (Da)	m/z	t_D	Average CCS ($Å^2$)	Std. Dev. ($Å^2$)
4	7716.36	1929.09	9.96	1025.12	2.82
5	7396.4	1479.28	5.66	938.52	4.57
6	7077.18	1179.53	3.64	879.26	6.67
7	6757.03	965.29	2.53	835.80	0.00
Average Experimental Collision Cross Sections (CCS) ($Å^2$)				919.68	±4.28
Theoretical Collision Cross Sections (CCS) ($Å^2$)				816.67	

*All drift times were collected at a travelling wave velocity of 350 m/s and a travelling wave height of 7.5 V.

[S1] Kaller, M.; Staffeld, P.; Haug, R.; Frey, W.; Giesselmann, F.; Laschat, S. *Liq. Cryst*. **2011**, *38*, 531–553.

[S2] Thalassinos, K.; Grabenauer, M.; Slade, S. E.; Hilton, G. R.; Bowers, M. T.; Scrivens, J. H. *Anal. Chem.* **2009**, *81*, 248-254.

[S3] Fernandez-Lima, F. A.; Blas, R. C.; Russell, D. H. *Int. J. Mass Spectrom.* **2010**, *298*, 111-118.

[S4] Jarosz, P.; Lotito, K.; Schneider, J.; Kumaresan, D.; Schmehl, R.; Eisenberg, R. *Inorg. Chem*. **2009**, *48*, 2420-2428.